Classical trajectory Monte Carlo model calculations for ionization of atomic hydrogen by 75-keV proton impact

L. Sarkadi*

Institute of Nuclear Research of the Hungarian Academy of Sciences (ATOMKI), H-4001 Debrecen, P.O. Box 51, Hungary

(Received 27 October 2010; published 30 November 2010)

Cross sections differential with respect to the energy loss and scattering angle of the projectile have been calculated for ionization of atomic hydrogen by 75-keV proton impact using the classical trajectory Monte Carlo method. The results are compared with the experimental data measured by Laforge *et al.* [Phys. Rev. Lett. **103**, 053201 (2009)] and Schulz *et al.* [Phys. Rev. A **81**, 052705 (2010)], as well as with the predictions of several quantum-mechanical theoretical models. The analysis of the deviations between the classical and the quantum-mechanical results shows that the three-body fragmentation dynamics cannot be understood purely classically; for the description of the process the quantum-mechanical treatment of the interplay between the electron-projectile and the projectile–target-nucleus interaction is unavoidable.

DOI: 10.1103/PhysRevA.82.052710 PACS number(s): 34.50.Fa, 34.10.+x

I. INTRODUCTION

The theoretical understanding of the collisional breakup of a three-body atomic system is one of the problems of fundamental importance in the physics of atomic collisions. Due to the difficulties arising from the long-range nature of the Coulomb force acting between the particles, no analytical solution of the Schrödinger equation exists for the process. The theoretical models worked out for the collisional breakup apply various approximations. In the absence of an exact solution to the problem, the only way to check the accuracy and the range of the validity of the models is the comparison of their predictions with experimental data. Consequently, experiments exploring the detailed dynamics of the three-body breakup are crucially important.

For ion-atom collisions the simplest collision process leading to three free particles in the final state is the ionization of the hydrogen atom by proton impact. In spite of the fundamental significance of the hydrogen atom as a target, due to the well-known difficulties of the cross section measurements for atomic hydrogen, the overwhelming majority of the ionization experiments were carried out for the hydrogen molecule, helium, and other heavier atoms and molecules. The experimental data obtained for nonhydrogenic targets greatly contribute to the understanding of the three-body dynamics, since the many-body problem of the single ionization of a few- (many-) electron target by impact of a bare nucleus can efficiently be reduced to a three-body problem by applying the "active electron" concept in the independent-electron approximation (see, e.g., [1]), particularly for small values of the perturbation parameter η (projectile-charge-to-collision-speed ratio) and for cases when total ionization cross sections or cross sections differential with respect of the energy and emission angle of the ejected electron are determined. However, from the ionization studies involving nonhydrogenic targets one can hardly draw firm and reliable conclusions for the three-body collision dynamics because of the uncertainty arising from the neglect of the correlation between the active and the passive electron(s). For molecular targets interference effects caused by the coherent electron emission from the atomic centers of the target [2] may also mask the details of the three-body collision dynamics.

Recently, Laforge *et al.* [3] and Schulz *et al.* [4] measured doubly differential cross sections for ionization of atomic hydrogen by 75-keV proton impact as a function of the projectile scattering angle and energy loss. In the experiment the projectile scattering angle θ_p covered a range from 0.05 to 0.95 mrad, the cross sections (denoted by DDCS_p) were determined for energy losses $\Delta E = 30$, 40, 50, and 53 eV. These experimental data are of particular importance, since according to the preceding general consideration they offer an accurate test of the three-body ionization theories. The authors compared their data with the predictions of various ionization models: The continuum-distorted-wave eikonal-initial-state (CDW-EIS) approximation [5,6], the three-body double-continuum Coulomb wave-functions (3C) description [7–9], and the so-called second-order Born approximation and Coulomb wave-function (SBA-C) model [10]. Two versions of the CDW-EIS model applying different corrections for the inclusion of the projectile–target-nucleus (PT) interaction were used in the comparison: CDW-EIS-SC and CDW-EIS-CL. The CDW-EIS-SC model accounts for the PT interaction semiclassically in terms of the eikonal approximation [11]. In the CDW-EIS-CL model, the PT interaction is accounted for by convoluting the CDW-EIS cross sections with the classical elastic scattering between the heavy particles using a Monte Carlo simulation [12–14]. (To avoid any confusion, we note that the Monte Carlo simulation made in the CDW-EIS-CL model has nothing to do with the CTMC method applied in the present work. The so-called Monte Carlo event generator proposed in works [12–14] is a tool for producing event files based on quantum-mechanical theories.) All the preceding models are perturbative approaches. The use of perturbation theory is justified, considering that for 75-keV proton impact the perturbation parameter is smaller than unity ($\eta = 0.58$).

In the CDW-EIS model higher-order contributions from the projectile-electron (PE) interaction are taken into account in the initial- and final-state wave function: The effect of the PE interaction in the final state is included by applying a distorted wave function for the ionized electron; in the initial state it is expressed by means of an eikonal phase factor. The

*sarkadil@atomki.hu

3C model is a kind of first Born approximation (FBA): The initial state and the transition operator agree with those of FBA, but the final state is a product of three Coulomb waves which, in addition to the description of the electron-target subsystem, describes also the PE and PT subsystems. The SBA-C model is an extension of the 3C model by including the PT interaction also in the transition operator. This model is, therefore, such a second Born approximation (SBA) in which the PT interaction is accounted for in both the transition operator and the final-state wave function. At higher collision velocities SBA-C converges to SBA.

The main conclusions drawn from the comparison of the predictions of the preceding models with the measured data of Laforge *et al.* [3] and Schulz *et al.* [4] can be summarized as follows. Surprisingly, for this rather simple collision system one can speak about only order-of-magnitude agreement between theory and experiment. Unexpectedly, the CDW-EIS-CL model, in which the correction for the PT interaction is treated classically, agreed better with the experiment than the CDW-EIS-SC model, where the same correction is treated semiclassically. The best overall agreement with the measurements (at least for the shape of the dependence of DDCS_p on θ_p) was observed for the SBA-C model. At the same time, for $\Delta E = 53$ eV the latter model resulted in a worse description than the 3C model. The energy-loss value, 53 eV, is special in that it corresponds to electron emission under the condition $v_e = v_p$ (v_e and v_p are the velocity of the ejected electron and the projectile, respectively). At $v_e = v_p$ strong postcollision interaction (PCI) takes place between the electron and the outgoing projectile, which leads to the appearance of the well-known cusp peak in the energy spectrum of the forward-ejected electrons. We note that here and in the following we assume that the energy loss of the projectile is directly related to the energy of the ejected electron because of the negligible recoil energy.

Keeping in mind that the cusp is a result of a *mutual* focusing effect between the outgoing projectile and the ejected electron, it is expected to be reflected in the energy and angular distribution of the scattered projectiles, too. Indeed, Schulz *et al.* [4] did find the sign of the focusing effect in the spectra of the scattered protons. DDCS_p exponentially falls with increasing θ_p. The rate of fall of the measured DDCS_p shows only a slight dependence on ΔE up to about 50 eV, but at 53 eV it suddenly increases; that is, the angular distribution of the scattered protons becomes narrower. Schulz *et al.* assumed that the sudden narrowing of DDCS_p at 53 eV is caused by the same PCI effect that produces the cusp in the spectrum of the forward-ejected electrons. Among the theories it is only the 3C model that shows a strong "narrowing effect" at $\Delta E = 53$ eV. We note that the narrowing was also observed in the angular distribution of the scattered projectiles in collisions of protons with helium atoms at the value of the energy loss corresponding to $v_e = v_p$ [15,16]. What is surprising is that the effect is much less pronounced for helium than for hydrogen.

In the theoretical interpretation of the experimental results several questions remained unanswered [3,4]: (i) Why does the CDW-EIS-CL model agree better with the experiment than the CDW-EIS-SC model? (ii) Why is the 3C model more successful than the other models in describing the narrowing effect at $\Delta E = 53$ eV? Considering that the SBA-C model is an extension of the 3C model, it is particularly surprising that the 3C model yields better result than the SBA-C model. (iii) Why is the narrowing effect much more stronger for hydrogen target than for helium target?

In this work we compare the experimental data of Laforge *et al.* [3] and Schulz *et al.* [4] with the results of calculations carried out in the framework of the classical trajectory Monte Carlo (CTMC) method. From the calculations we hoped to get at least partial answers to some of the preceding questions. The CTMC method is complementary to the existing quantum-mechanical descriptions for the following reason. Although the fulfillment of the condition $\eta < 1$ for the present collision system allows the use of perturbation theories, η is not so small, and doubt may arise about the convergence of the applied models. Unfortunately, at present nonperturbative quantum-mechanical three-body ionization theories that account for all the interactions between the particles (even up to asymptotically large separation distances) do not exist. The great advantage of the CTMC method in this respect is that it is a nonperturbative theory; that is, it describes the full three-body dynamics exactly in the framework of the classical mechanics. The comparison of the CTMC results with those obtained by the quantum-mechanical calculations gives a possibility to separate off those features of the three-body dynamics which cannot be understood on the basis of a classical picture.

In the present work we mainly focus on the narrowing effect. Our CTMC results for DDCS_p show an enhancement of the cross section at the energy loss corresponding to $v_e = v_p$ rather than narrowing of the angular distribution of the scattered protons. Since one expects a narrowing effect in the classical view of the Coulomb focusing, at first glance this finding is surprising. We present a detailed analysis of the three-body dynamics in which we resolve the apparent discrepancy. In the examples of individual projectile trajectories we discuss the effect of the PT interaction in the ionization process and suggest some quantum-mechanical effects that may explain the experimentally observed behavior of DDCS_p.

II. THEORETICAL METHOD

The CTMC method is based on the numerical solution of the classical equations of motion for a large number of trajectories of the interacting particles under randomly chosen initial conditions [17,18]. Our computer code solves Newton's nonrelativistic equations of motion for the three particles (in atomic units):

$$m_i \frac{d^2\mathbf{r}_i}{dt^2} = \sum_{j(\neq i)=1}^{3} Z_i Z_j \frac{\mathbf{r}_i - \mathbf{r}_j}{|\mathbf{r}_i - \mathbf{r}_j|^3}, \quad (i = 1,2,3). \qquad (1)$$

Here m_i, Z_i, and $\mathbf{r}_i$ are the masses, charges, and position vectors of the particles, respectively. The randomly selected initial conditions were the impact parameter and five further parameters defining the position and velocity vector of the target electron moving in Kepler orbits. The ranges of the latter parameters were constrained to give the binding energy of the hydrogen atom, 0.5 a.u. For the generation of the initial values of the position and velocity coordinates of the electron from a set of uniformly distributed variables we applied the

general procedure suggested by Reinhold and Falcón [19] for non-Coulombic systems, which is equivalent to the original Abrines and Percival's method [17] in the case of the Coulomb interaction.

The integration of the equations of motion was started at a large distance (200 a.u.) between the incoming proton and the hydrogen atom. This was necessary for the accurate determination of the energy loss of the projectile. After the collision the calculations were made in two steps. In the first step the integration was continued until the internuclear distance $R = 200$ a.u., where the main reaction channels (excitation, ionization, charge transfer) could be identified safely. In the second step only collision events leading to ionization were regarded. Considering the slow convergence of the cross section for the formation of the electron cusp as a function of the internuclear distance [20,21], in the second step the trajectories of the particles were calculated up to $R = 10^8$ a.u.

The doubly differential cross section describing the energy and angular distribution of the ith particle following the fragmentation (in short notation DDCS_i) is classically expressed as

$$\frac{d^2\sigma}{d\epsilon_i d\Omega_i} = 2\pi \int_0^\infty b \frac{d^2P}{d\epsilon_i d\Omega_i}(b) db, \tag{2}$$

where $d^2P/d\epsilon_i d\Omega_i$ is doubly differential ionization probability of the process and b is the impact parameter. One can easily show that for a large number of collision events characterized by uniformly distributed b values in the range $(0, b_{\max})$ the integral in (2) can be approximated by the following sum:

$$\int_0^\infty b \frac{d^2P}{d\epsilon_i d\Omega_i}(b) db \approx \frac{b_{\max} \sum_j b_j^{(i)}}{N \Delta\epsilon_i \Delta\Omega_i}. \tag{3}$$

Here $b_j^{(i)}$ is the actual impact parameter at which the fragment is scattered to the energy window $\Delta\epsilon_i$ and solid angle window $\Delta\Omega_i$. Due to the azimuthal symmetry, $\Delta\Omega_i$ is determined by the polar angular window ranging from $\theta_i^{\min}$ to $\theta_i^{\max}$:

$$\Delta\Omega_i = \int_0^{2\pi} \int_{\theta_i^{\min}}^{\theta_i^{\max}} \sin\theta d\theta d\phi = 2\pi \left(\cos\theta_i^{\min} - \cos\theta_i^{\max} \right). \tag{4}$$

From Eqs. (2)–(4) we obtain

$$\frac{d^2\sigma}{d\epsilon_i d\Omega_i} \approx \frac{b_{\max} \sum_j b_j^{(i)}}{N \left(\cos\theta_i^{\min} - \cos\theta_i^{\max} \right) \Delta\epsilon_i}. \tag{5}$$

For DDCS_p the energy loss of the protons is expressed as $\Delta E = E - \epsilon_p$, where E is the impact energy, and ϵ_p is the energy of the scattered proton. Therefore, DDCS_p denotes the cross section

$$\mathrm{DDCS}_p \equiv \frac{d^2\sigma}{d\Omega_p d(\Delta E)}(\theta_p, \Delta E). \tag{6}$$

In our calculations we followed the history of altogether 1.3×10^8 collision events in the impact parameter range between 0 and 4 a.u. For the total cross section of the ionization of the hydrogen atom by impact of 75-keV protons we obtained a slightly higher value (1.45×10^{-16} cm^2) than the recommended value (1.27×10^{-16} cm^2) based on a large collection of experimental data [22].

III. RESULTS AND DISCUSSION

Figure 1 presents our CTMC results for DDCS_p as a function of the scattering angle θ_p at fixed values of the energy loss, $\Delta E = 30$, 40, 50, and 53 eV. In the figure are also plotted the experimental data and the predictions of the ionization models discussed in Sec. I. In calculation of the cross sections, in Eq. (5) we used a value of 3 eV for the energy window. The bin size of the scattering angle was 0.05 mrad for $\theta_p < 0.5$ mrad, and it was 0.1 mrad for larger values of θ_p. These values were chosen in accordance with the energy and angular resolution of the experiment.

CTMC describes well the main tendencies of the experimental data. However, one can speak about good agreement only at large scattering angles ($\theta_p > 0.6$ mrad), except for the case of $\Delta E = 53$ eV, where, at the same time, the observed rapid fall of DDCS_p is quite uncertain due the large errors of the data and the lack of measuring points at $\theta_p \geqslant 0.8$ mrad. At low and medium values of θ_p the CTMC model cannot reproduce the observed shape of DDCS_p as a function of θ_p. Particularly, our calculations do not account for the bump seen in the experimental data at $\theta_p \approx 0.4$ mrad. Comparing with the other theoretical models, the CTMC description shows a great similarity with the CDW-EIS-SC model, at medium values of θ_p the agreement between the two theories is almost perfect. This is surprising because one would expect better agreement with the CDW-EIS-CL model that includes a classical correction for the PT interaction.

As far as the narrowing effect is concerned, the CTMC method fails to reproduce the enhancement of DDCS_p at small values of θ_p and the sudden change in the rate of fall of the data for the spectrum measured at $\Delta E = 53$ eV. Schulz *et al.* [4] investigated the narrowing effect by plotting the average proton scattering angle θ_{avg} as a function of v_e/v_p. In Fig. 2 we reproduced the θ_{avg} data obtained by the authors, and in addition we plotted also the predictions of the various theoretical models. As is seen from the figure, the CTMC method predicts only a small change in the slope of the θ_{avg} curve at $v_e/v_p \approx 1$. Among the theories it is only the 3C model that shows a drastic drop of θ_{avg} in accordance with the experiment. We note that similar narrowing effect was also observed for ionization of molecular hydrogen at the same collision energy [23] (see the corresponding data points in Fig. 2).

Our finding that the CTMC method does not show the narrowing effect at $\Delta E = 53$ eV is unexpected because of the reason discussed in Sec. I. To analyze the properties of DDCS_p in more detail, in Fig. 3(a) we displayed our CTMC results in a three-dimensional plot. The effect of PCI between the outgoing protons and the ejected electrons is reflected in the distribution of DDCS_p in the form of a small, broad peak centered at $\Delta E \approx 53$ eV. The peak appears within a small range of the scattering angle ($\theta_p < 0.2$ mrad), and therefore, practically, it does not change the width of the angular distribution. The fact that the effect of PCI on DDCS_p is so small is surprising considering that the same effect leads to a very pronounced cusp in the doubly differential spectrum of the ejected electrons

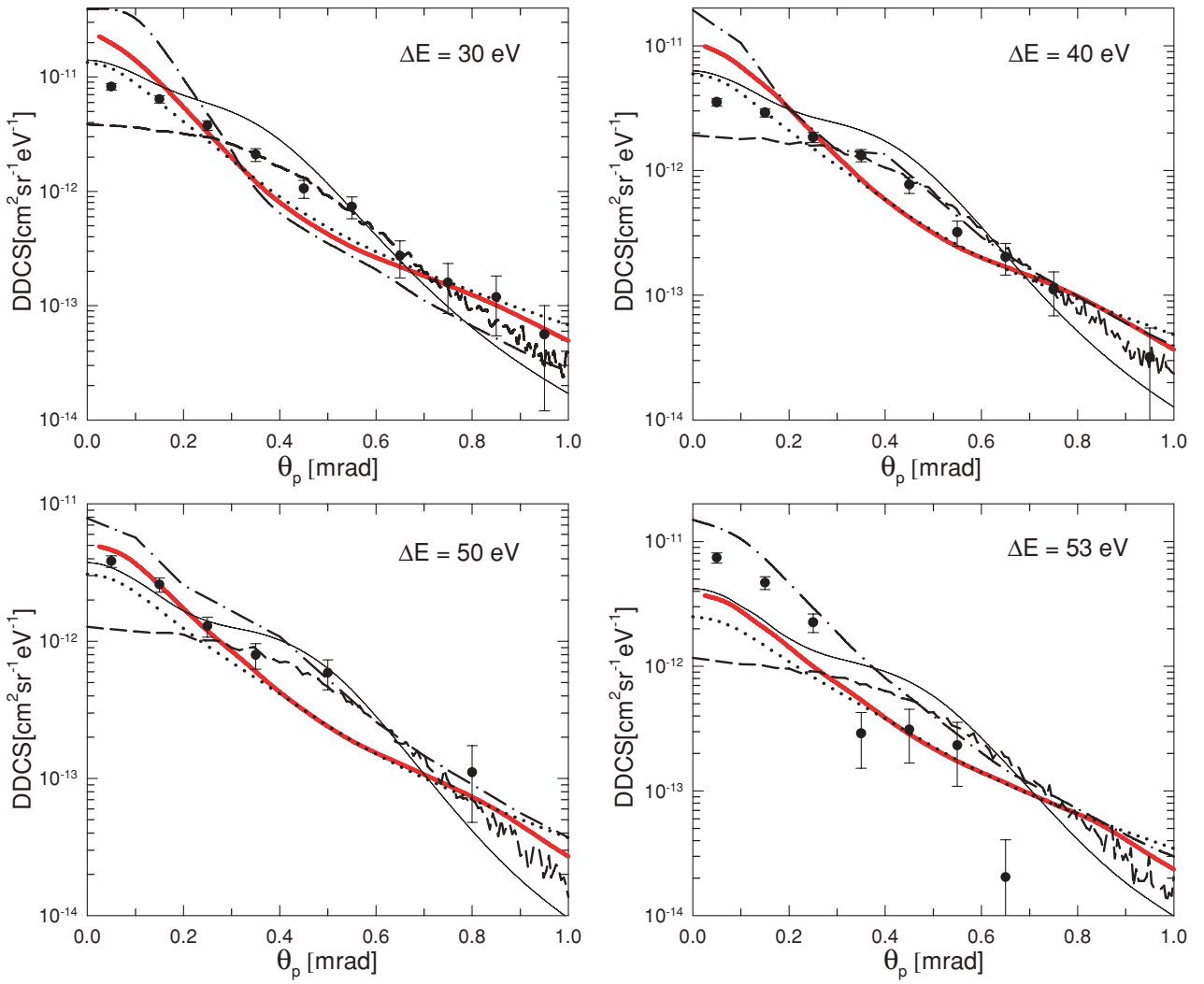

FIG. 1. (Color online) Doubly differential cross sections for a 75-keV proton on hydrogen collisions as functions of the proton scattering angle at fixed values of the energy loss. The experimental data are from measurements by Laforge *et al.* [3] and Schulz *et al.* [4]. The notations of the theories: thick solid (red) curves, CTMC; dotted curves, CDW-EIS-SC; dashed curves, CDW-EIS-CL; dash-dotted curves, 3C; thin solid curves, SBA-C.

(see Fig. 4). The different manifestation of the PCI effect in DDCS_p and DDCS_e can be explained as follows. The $v_e = v_p$ peak in DDCS_p is superimposed on a large "background" of ionization events in which the proton scatters at a small angle ($\theta_p < 1$ mrad), but the electron is ejected with an angle that lies outside the range in which the cusp is observable. For such events PCI is small, and thereby the corresponding DDCS_p values have a smooth distribution. To verify this assumption, we calculated DDCS_p with the condition that only those events were considered in which the electrons were ejected into forward direction ($\theta_e < 5^\circ$). The result is shown in Fig. 3(b). Now the PCI effect is much more pronounced, but it appears as a long ridge rather than a peak. Analyzing the ridge structure in Fig. 3(b), one can establish that any sections of the distribution at a given value of θ_p are of similar shape; that is, the effect of PCI on the energy (loss) spectrum of the scattered protons is practically independent from the scattering angle. This suggests the picture that PCI and the scattering of the projectile (either on the electron or the target nucleus, or on both particles) are separable processes. The separability is in accordance with the widely accepted view of the cusp formation: While the scattering is characterized by the time by which the projectile passes through the atom, the cusp is formed as a result of a long-time final-state interaction. We note that in one of our previous experiments carried out for 75-keV proton on argon collisions [24] we observed the electron cusp even for large scattering angles of the protons (up to $\theta_p = 8.1^\circ$). The cusp was observed at $\theta_e = \theta_p$, supporting the picture that it is a result of final-state interaction.

A question arises: How can one determine the part of DDCS_p that can be attributed purely to PCI? This can be done considering that the cusp is dominantly formed by *mutual* interaction between the electron and the projectile at asymptotically large internuclear distances in the outgoing phase of the collision. Although the cusp formation is affected by the receding target ion, to a good approximation it is a two-body mechanism. This holds also at large scattering angles: The scattered projectile focuses the ejected electron

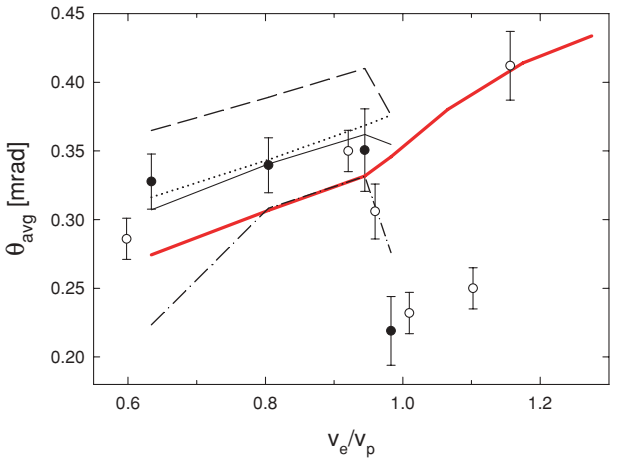

FIG. 2. (Color online) Average scattering angle of the proton as a function of the ratio of the ejected electron velocity v_e to the projectile velocity v_p. Experimental data: solid circles, atomic hydrogen target [4]; open circles, molecular hydrogen target [23]. For the notations of the theoretical curves, see Fig. 1. (All the calculations refer to atomic hydrogen target.)

in the direction of the scattering. Since the mutual interaction between the two particles does not affect the motion of their center-of-mass (c.m.), the scattering process can be separated off by measuring the scattering angle of the projectile relative to the direction of the c.m. velocity vector of the electron-projectile subsystem, $\mathbf{v}_{\text{c.m.}}$. It is expected that the distribution of the relative scattering angle, denoted by θ'_p, reflects the cusp formation better than that of the laboratory angle, θ_p.

Figure 5 displays our CTMC results for the cross section

$$\text{DDCS}'_p = \frac{d^2\sigma}{d\Omega'_p d(\Delta E)}(\theta'_p, \Delta E), \tag{7}$$

calculated in the same way as DDCS_p with use of Eq. (5) but with the relative scattering angle θ'_p. The distribution shows a pronounced peak at $\Delta E = 53$ eV, as is expected. Since the peak has a sharp, cusplike shape, the distribution of θ'_p is narrower at $\Delta E = 53$ eV than at other values of the energy loss. It is important to note that the peak is restricted in a small range of θ'_p; it practically disappears at $\theta'_p = 0.1$ mrad. From the momentum exchange between the proton and the electron one can estimate that $\theta'_p = 0.1$ mrad corresponds to an electron ejection angle $\theta_e \approx \theta'_e \approx (M/m)\theta'_p \approx 10^\circ$ (here m and M are the masses of the electron and the proton, respectively). This is in accordance with the fact that the electron cusp is restricted to the angular range $\theta_e < 10^\circ$.

A detailed mathematical analysis of DDCS_p with consideration to the separability of the primary proton scattering and PCI between the outgoing electron and proton is given in the Appendix.

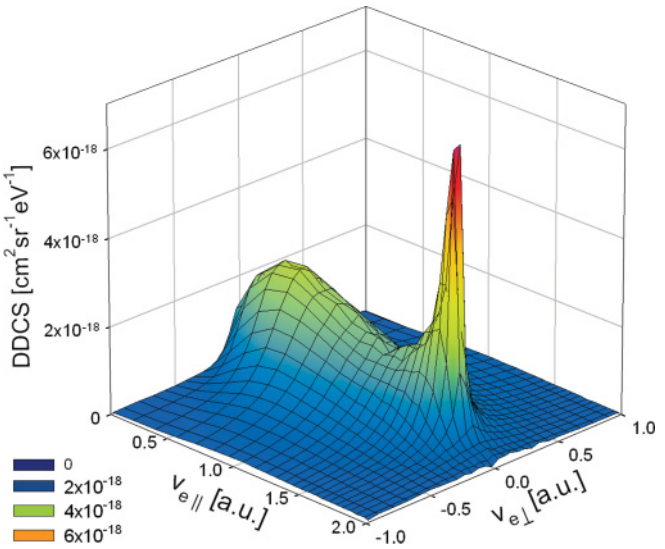

FIG. 4. (Color online) $d^2\sigma/d\epsilon_e d\Omega_e$ for electron ejection in a 75-keV proton on hydrogen collisions obtained from the present CTMC calculations. $v_{e\|}$ and $v_{e\perp}$ are the parallel and perpendicular components, respectively, of the velocity vector of the electron with respect of the initial velocity vector of the projectile.

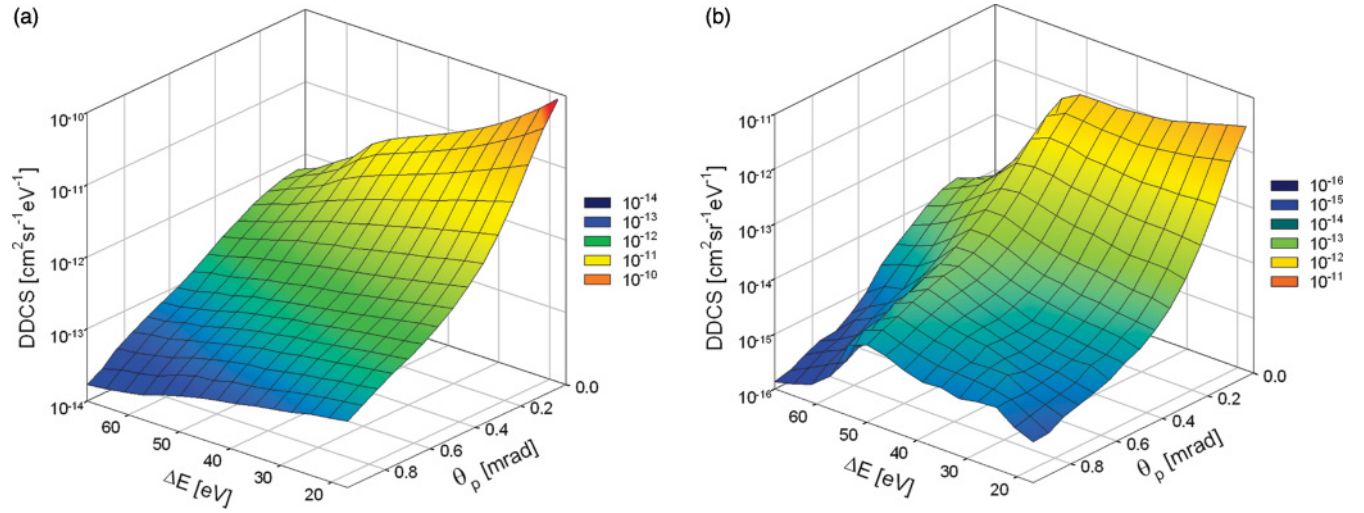

FIG. 3. (Color online) Three-dimensional representation of DDCS_p obtained from the present CTMC calculations. (a) Inclusive DDCS_p with respect to the emission angle of the ejected electron. (b) DDCS_p calculated with the condition $\theta_e < 5^\circ$.

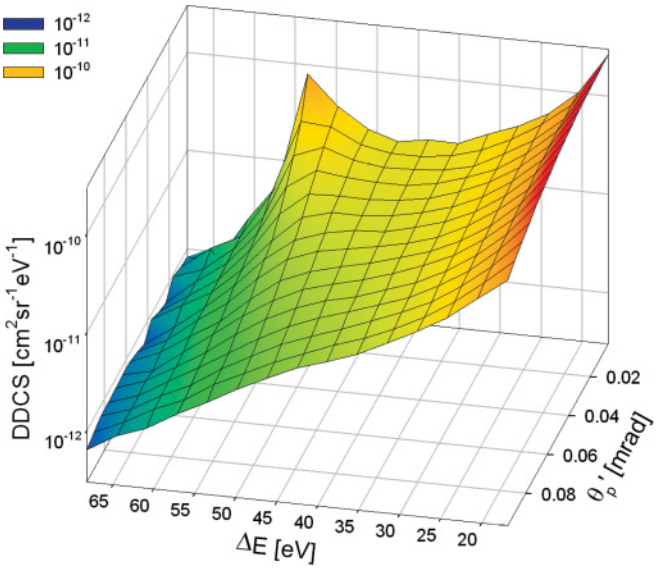

FIG. 5. (Color online) Result of the calculations for the $d^2\sigma(\theta'_p,\Delta E)/d\Omega'_p d(\Delta E)$ distribution. The scattering angle θ'_p is measured relative to the direction of the center-of-mass velocity vector of the electron-projectile subsystem.

From the CTMC results we may conclude that in a *classical* description of the ionization process the narrowing effect is not expected to appear in DDCS_p (if it is an inclusive cross section with respect to the emission of the electron). However, then the question is why is it reflected in the experimental data as well as in the predictions of the 3C theoretical model?

The discrepancy between the CTMC method and the experiment indicates that the observed properties of DDCS_p can only partly be understood classically. Searching for possible quantum-mechanical effects, we investigated the role of the nucleus-nucleus (PT) interaction in the dynamics of the ionization process. We run our CTMC code without including the PT interaction. The results are shown in Fig. 6. Dramatic differences as compared with the corresponding distributions

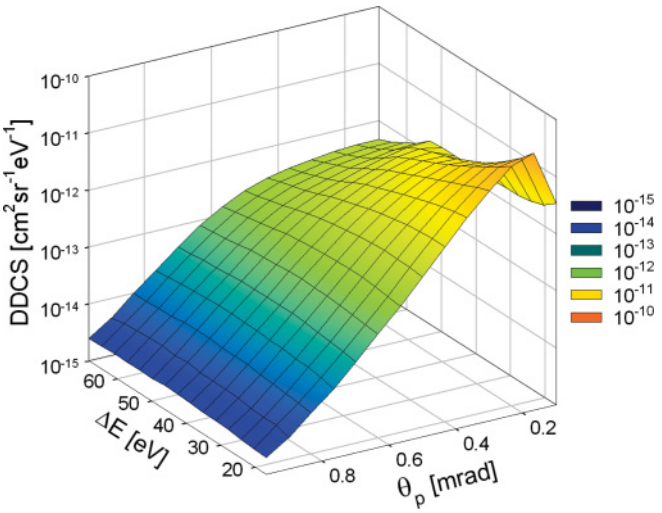

FIG. 6. (Color online) DDCS_p calculated with neglect of the nucleus-nucleus interaction.

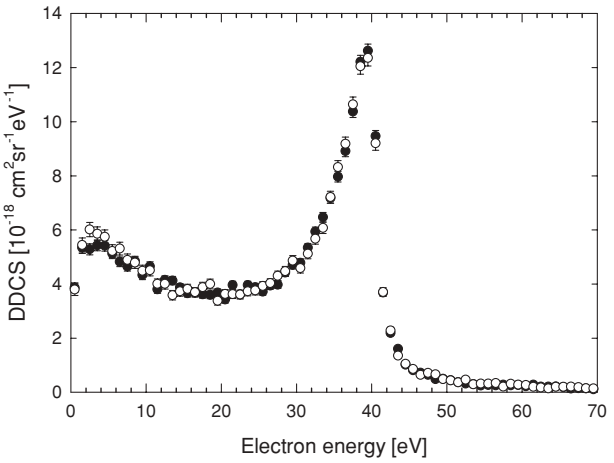

FIG. 7. Energy spectrum of the forward-ejected electrons ($\theta_e < 2^\circ$) calculated with (open circles) and without (solid circles) the inclusion of the PT interaction.

in Fig. 3(a) can be observed, particularly at small θ_p values. At the same time, the electron cusp is hardly affected by the inclusion of the PT interaction (see Fig. 7). This can be understood simply by considering that the change of the proton scattering angle due to the PT interaction is typically in the mrad region; therefore, θ_p remains in a range that is still $\approx 0^\circ$ from the point of view of the electron emission.

For a further, more detailed analysis of the role of the nucleus-nucleus scattering, in Fig. 8(a) we plotted our CTMC results obtained for DDCS_p with and without the inclusion of the PT interaction (the latter one is denoted by CTMC-noPT) as a function of θ_p at a specific value of ΔE (50 eV). The steep decrease of the CTMC-noPT results above $\theta_p \approx 0.5$ mrad can be understood by considering the scattering of the proton on a free, stationary electron. For a binary collision there is a one-to-one relationship between the scattering angle and the energy loss of the projectile. From the momentum and energy conservation one obtains, to a good approximation,

$$\sin\theta_p \approx \left[\frac{\Delta E}{E}\left(\frac{m}{M} - \frac{1}{4}\frac{\Delta E}{E}\right)\right]^{1/2}. \tag{8}$$

In the range of the energy loss considered for this collision system this formula yields values between 0.42 and 0.51 mrad. The occurrence of scattering angles smaller or larger than the *binary encounter* (BE) angle given by Eq. (8) at a fixed value of ΔE is due to the initial velocity distribution of the bound electron. As is expected, the inclusion of the PT interaction increases the probability of the large-angle scatterings in the ionization. However, it is not so obvious why it enhances the cross section at small θ_p values, too. To investigate this effect, we plotted large number of calculated individual particle trajectories for collision events that terminated with small-angle scattering. One of the plots showing the projectile's trajectory for a collision leading to $\theta_p = 0.1$ mrad is seen in Fig. 9(a). The trajectory has a zig-zag shape: The large-angle PE scattering is compensated by a subsequent PT scattering, resulting in a small final θ_p value. Without the PT interaction the projectile would scatter at a much larger angle, $\theta_p = 0.4$ mrad. The occurrence of such trajectories shifts a part of the collision events from the range $0.2 < \theta_p < 0.6$ mrad to the

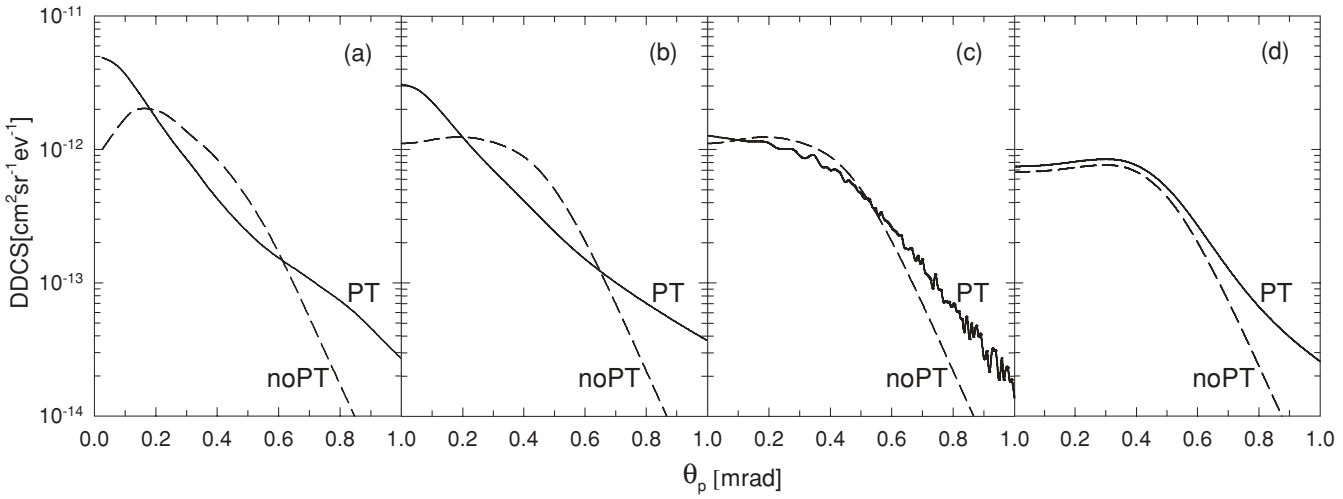

FIG. 8. Theoretical results for DDCS$_p$ as a function of the proton scattering angle at a fixed energy-loss value (50 eV). The solid and dashed curves denote calculations carried out with and without inclusion of the nucleus-nucleus scattering, respectively. (a) CTMC and CTMC-noPT; (b) CDW-EIS-SC and CDW-EIS-noPT [4]; (c) CDW-EIS-CL and CDW-EIS-noPT; (d) SBA and FBA [4].

range $\theta_p < 0.2$ mrad, thereby increasing (reducing) the cross section at small (medium) scattering angles.

As a result of the inclusion of the PT interaction, the curvature of the CTMC-noPT line in Fig. 8(a) changes from convex to concave shape. Similarly, the CDW-EIS model predicts a convex shape for the dependence of DDCS$_p$ on θ_p, and the inclusion of the PT interaction in the CDW-EIS-SC model results in also a concave shape [see Fig. 8(b)]. This similarity indicates that the treatment of the PT interaction in the CDW-EIS-SC model by the eikonal approximation is a correct procedure in that it is able to account for the previously discussed effect of the zig-zag-shaped projectile trajectories on DDCS$_p$. In contrast to this, the latter effect is poorly reflected by CDW-EIS-CL: The classical correction for the inclusion the nucleus-nucleus scattering modifies the cross section significantly only at large scattering angles; therefore, the shape of the CDW-EIS-CL remains convex [see Fig. 8(c)].

According to Fig. 8(a), CTMC predicts a considerable effect of the PT interaction on DDCS$_p$ at medium θ_p values (a *decrease* by a factor of about two at $\theta_p \approx 0.4$ mrad). The CDW-EIS-SC model supports this finding. Surprisingly, the comparison between the FBA and SBA results in Fig. 8(d) shows that the inclusion of the nucleus-nucleus scattering results in only the *increase* of DDCS$_p$. It is an interesting question whether perturbation theories are able to predict the decrease of DDCS$_p$ found in the classical and semiclassical descriptions and explained by the occurrence of zig-zag-shaped projectile trajectories. To investigate this question, let us consider the form of the scattering amplitude in SBA (see, e.g., [25]). In atomic units,

$$f^{\mathrm{Born2}} = f^{\mathrm{B1}} + f^{\mathrm{B2}}, \tag{9}$$

where f^{B1} is the first Born term,

$$f^{\mathrm{B1}} = -\frac{1}{2\pi}\langle \mathbf{k}_f \psi_f | V | \mathbf{k}_0 \psi_0 \rangle, \tag{10}$$

and f^{B2} is the second Born term,

$$f^{\mathrm{B2}} = -\frac{\mu}{8\pi^4} \lim_{\lambda \to 0+} \sum_n \int d\mathbf{k} \langle \mathbf{k}_f \psi_f | V | \mathbf{k} \psi_n \rangle \times \frac{\langle \mathbf{k} \psi_n | V | \mathbf{k}_0 \psi_0 \rangle}{k_n^2 - k^2 + i\lambda}. \tag{11}$$

In the preceding expressions $\langle \mathbf{k}_p \psi_p | V | \mathbf{k}_q \psi_q \rangle$ denotes the following matrix element:

$$\langle \mathbf{k}_p \psi_p | V | \mathbf{k}_q \psi_q \rangle \equiv Z_p \langle e^{i\mathbf{k}_p \mathbf{R}} \psi_p(\mathbf{r}) | \left(\frac{1}{R} - \frac{1}{|\mathbf{R} - \mathbf{r}|} \right) | e^{i\mathbf{k}_q \mathbf{R}} \psi_q(\mathbf{r}) \rangle. \tag{12}$$

In Eqs. (10)–(12) Z_p is the charge of the projectile and μ is the reduced mass of the projectile-atom system. $\mathbf{R}$ and $\mathbf{r}$ are the position vector of the projectile and the electron, respectively. ψ_0 is the initial ground state and ψ_f is the final ionized state of the hydrogen atom. In Eq. (11) the summation is over all eigenstates ψ_n of the target, including the continuum states. The vectors $\mathbf{k}_0$, $\mathbf{k}_f$ and the quantity k_n are defined by

$$\begin{aligned} \mathbf{k}_0 &= \mu \mathbf{v}_0, \\ \mathbf{k}_f &= \mu \mathbf{v}_f, \\ k_n^2 &= k_0^2 + 2\mu(\epsilon_0 - \epsilon_n). \end{aligned} \tag{13}$$

Here $\mathbf{v}_0$ ($\mathbf{v}_f$) is the initial (final) velocity of the projectile relative to the target, and ϵ_n is the eigenenergy of the state ψ_n.

DDCS$_p$ is obtained by integration of $|f^{\mathrm{Born2}}|^2$ over the electron emission angle,

$$\frac{d^2\sigma^{\mathrm{Born2}}}{d\Omega_p d(\Delta E)} \propto \int_{4\pi} |f^{\mathrm{Born2}}|^2 d\Omega_e = \int_{4\pi} |f^{\mathrm{B1}} + f^{\mathrm{B2}}|^2 d\Omega_e. \tag{14}$$

Using the orthogonality property of the eigenstates ψ_n, f^{B1} and f^{B2} can be expressed in the forms:

$$f^{\mathrm{B1}} = -\frac{1}{2\pi}\langle \mathbf{k}_f \psi_f | V_{\mathrm{PE}} | \mathbf{k}_0 \psi_0 \rangle, \tag{15}$$

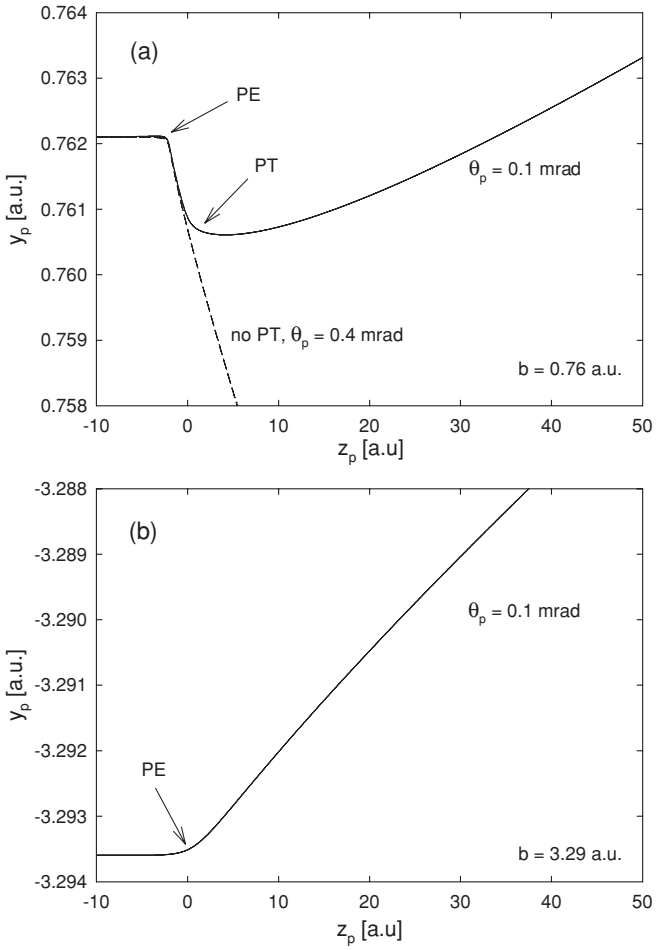

FIG. 9. Samples of projectile trajectories obtained by the present CTMC calculations. The z axis is defined by the initial velocity vector of the projectile. (a) Trajectory affected strongly by both the PE and the PT interaction. (b) Trajectory characterized by dominant PE interaction. The two trajectories belong to collisions of the same final state ($\theta_p = 0.1$ mrad, $\theta_e = 0^\circ$, and $\Delta E = 50$ eV). In panel (a) the trajectory shown by the dashed curve was obtained neglecting the PT interaction.

and

$$f^{\mathrm{B2}} = -\frac{\mu}{8\pi^4}\lim_{\lambda\to 0+}\left(\int d\mathbf{k}\langle \mathbf{k}_f\psi_f|V_{\mathrm{PE}}|\mathbf{k}\psi_0\rangle\frac{\langle \mathbf{k}\psi_0|V_{\mathrm{PT}}|\mathbf{k}_0\psi_0\rangle}{k_0^2-k^2+i\lambda}\right.$$
$$+\int d\mathbf{k}\langle \mathbf{k}_f\psi_f|V_{\mathrm{PT}}|\mathbf{k}\psi_f\rangle\frac{\langle \mathbf{k}\psi_f|V_{\mathrm{PE}}|\mathbf{k}_0\psi_0\rangle}{k_f^2-k^2+i\lambda}$$
$$\left.+\sum_n\int d\mathbf{k}\langle \mathbf{k}_f\psi_f|V_{\mathrm{PE}}|\mathbf{k}\psi_n\rangle\frac{\langle \mathbf{k}\psi_n|V_{\mathrm{PE}}|\mathbf{k}_0\psi_0\rangle}{k_n^2-k^2+i\lambda}\right), \quad (16)$$

with the notations $V_{\mathrm{PE}} = -Z_p/|\mathbf{R}-\mathbf{r}|$ and $V_{\mathrm{PT}} = Z_p/R$.

The only nonvanishing matrix elements of the PT interaction occur in the f^{B2} amplitude, in the first and second term of Eq. (16). The first term describes a process in which the proton elastically scatters on the target nucleus while the atom is in the ground state, and then it ejects the electron (PT-PE sequence). The interpretation of the second term: First the proton ionizes the atom and then elastically scatters on the nucleus of the ionized target atom (PE-PT sequence). For example, the trajectory shown in Fig. 9(a) is a result of PE-PT sequence. Since such zig-zag-shaped trajectories lead to small scattering angles, SBA is able to account for the increase of DDCS$_p$ at low θ_p values. Scatterings (in either PT-PE or PE-PT sequence) into directions of the same sign may lead to large scattering angles; that is, the SBA model describes the increase of DDCS$_p$ also at large θ_p values. As far as the medium θ_p values are concerned, the SBA model cannot account for the decrease of DDCS$_p$ for the following reason. As discussed earlier, the drop of DDCS$_p$ in the medium range of θ_p classically can be interpreted by the fact that due to the increasing role of the nucleus-nucleus interactions for $\theta_p > 0.4$ mrad, part of the collision events "scatters out" from the range $0.2 < \theta_p < 0.6$ mrad. The Born approximation cannot describe consistently the decrease of the scattered particle flux, because it is not a unitary theory (the flux is not conserved). Particularly considering the relatively large value of the perturbation parameter ($\eta = 0.58$), the SBA results have to be accepted with caution. The PT interaction can consistently be treated by a nonperturbative unitary theory that takes into account the *channel interactions* between the scatterings of the projectile into different angles.

In the SBA-C model the effect of PCI between the outgoing proton and electron is included by taking the final-state wave function in the form of the product of three Coulomb waves. The inclusion of PCI enhances DDCS$_p$ at small θ_p values. As a result, an inflection point and a bump appear on the SBA-C curves in Fig. 1 at $\theta_p \approx 0.2$ mrad and $\theta_p \approx 0.4$ mrad, respectively. We note that the position of the bump reflects the previously discussed BE angle, $\theta_p \approx 0.4$–0.5 mrad (the scattering angle for the collision of a proton with a free, stationary electron). At the BE angle the FBA curve has a shoulder that remains practically unchanged after the second-order correction, and this shoulder together with the enhanced DDCS$_p$ at small θ_p values lead to the bump for the SBA-C curve.

The bump predicted by the SBA-C model is more pronounced than the observed one; for $\Delta E = 30$, 40 and 50 eV the measured data lie halfway between the CTMC and SBA-C curves in the range $0.3 < \theta_p < 0.6$ mrad. Focusing on this θ_p range, we may assume that the difference between the measured DDCS$_p$ data and the CTMC results is a quantum-mechanical effect, which in turn is overestimated by the SBA-C model. The reasons why the latter model predicts too large cross sections were mentioned earlier: the nonunitarity of the perturbation theory and the neglect of the channel interactions. There is a further effect that explains the convex curvature reflected in the tendencies of the measured data in contrast to the concave curvature of the CTMC curves. As we discussed earlier, the concave shape of the CTMC curves can be traced back to the decrease of the collision events in the medium θ_p range due to the increasing role of the nucleus-nucleus interaction for $\theta_p > 0.4$ mrad. At the same time, besides the "scattering-out" events, there is some contribution from the "scattering-in" events that increases the cross section in the range $0.3 < \theta_p < 0.6$ mrad. The final concave curvature of the CTMC curves is a result of a dynamical equilibrium between the scattering-in and scattering-out processes.

The quantum-mechanical treatment of the equilibrium may lead to a different result for the following reason. In the considered range of θ_p part of the ionization collisions

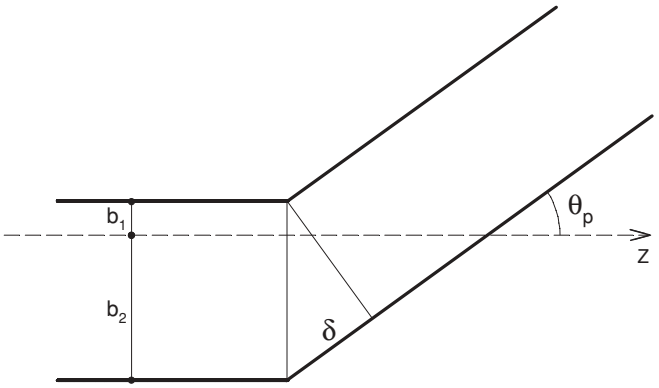

FIG. 10. Geometry of the path interference. The two trajectories are of the types plotted in Fig. 9.

proceed practically without nucleus-nucleus scattering, and part of them are strongly affected by the PT interaction. The scattering-in events belong to the latter category. In SBA the ionization without (with) PT is described by the first (second) Born amplitude. A *constructive interference* between the two amplitudes in Eq. (14) may lead to a larger cross section than the classical result. In other ranges of θ_p the interference may be destructive, leading to a smaller cross section than the classical one. Figure 9(b) shows a projectile trajectory characterized by the same scattering angle as that in Fig. 9(a) ($\theta_p = 0.1$ mrad), but in contrast to the latter, it belongs to a collision that proceeds with a negligible nucleus-nucleus scattering. In both collisions the electron is ejected in the same direction ($\theta_e = 0^\circ$) and with the same energy ($\Delta E =$ 50 eV), that is, the final states of the two collisions are indistinguishable; therefore, their amplitudes may interfere. The interference may be destructive, which would explain why the CTMC method overestimates the measured cross sections for $\theta_p < 0.2$ mrad and $\Delta E = 30, 40$, and 50 eV. In the followings we show that the kinematics of the collision allows such a "path interference." Figure 10 depicts the geometry of two trajectories of the same types as those in Fig. 9. For the sake of simplicity we assume coplanar scatterings. In this case the path difference between the trajectories is $\delta = (b_1 + b_2) \sin\theta_p$. For example, let us consider the condition of the constructive interference: $\delta = n\lambda$ ($n = 1,2, \ldots$), where λ is the de Broglie wavelength of the scattered proton. For 75-keV protons, $\lambda = h/Mv_p \approx h/Mv_0 = 1.97 \times 10^{-3}$ a.u. With the choice $n = 1$ from the preceding condition we obtain $b_1 + b_2 = 1.97 \times 10^{-3}/\sin\theta_p$ a.u. $\approx 1.97 \times 10^{-3}/\theta_p$ a.u. Considering that the range of θ_p is between 0.1 and 1 mrad, the corresponding range of the $b_1 + b_2$ is between 2 and 20 a.u. This range is of the same order of magnitude as the impact parameter range of the ionization. For example, for the trajectories in Fig. 9, $b_1 + b_2 = 4.05$ a.u. Consequently, path interference effects may influence the angular distribution of the scattered protons significantly.

The preceding analysis shows that the path interference is very sensitive to the kinematics of the collision. Since PCI between the ejected electron and the scattered proton modifies the kinematics to the largest extent at $\Delta E = 53$ eV, strong interference effects are expected to occur at this energy loss value. A constructive interference may significantly enhance the small PCI effect obtained in our CTMC calculations at small θ_p values; a destructive interference may decrease DDCS_p at medium and large values of θ_p. This would explain the experimentally observed narrowing of the angular distribution of the scattered protons. However, we stress that the narrowing is a result of a quantum-mechanical interplay between the ionization induced by the PE interaction and the nucleus-nucleus scattering and cannot be interpreted as a *direct* manifestation of the mutual Coulomb focusing between the equivelocity outgoing electron and proton.

The possible interference effects in the projectile scattering increase the complexity of the problem further and make it difficult to answer the questions mentioned in Sec. I. It is hard to follow how and to what extent the different approximations applied in the higher-order theories (SBA-C, 3C) change the relative weight and phase of the f^{B1} and f^{B2} amplitudes in Eq. (9) and thereby lead to a weaker or stronger interference effect in a specific range of θ_p and at a given value of ΔE. Furthermore, due to the uncertainty concerning the convergence of the Born series, question (ii) in Sec. I has not much meaning: One cannot exclude that the observed good performance of the 3C model in describing the narrowing effect at $\Delta E = 53$ eV is only accidental. As far as question (iii) is concerned, the smaller narrowing effect observed for helium target can be understood partly classically: For a heavier target, the increased probability of the nucleus-nucleus scattering washes out the PCI effect in a larger extent. Quantum mechanically, the stronger PT interaction increases the relative weight of the f^{B2} amplitude, leading to an altered interference between f^{B1} and f^{B2}.

IV. CONCLUSIONS

In the present work we investigated theoretically the narrowing effect occurring in the angular distribution of the scattered projectiles in ionizing collisions as a result of the mutual focusing effect between the forward-ejected electron and the outgoing projectile at the velocity-matching condition, $v_e = v_p$. For the study of the problem we carried out CTMC calculations for 75-keV protons on hydrogen collisions. The obtained results show the narrowing effect, but only in that case when the scattering angle of the projectile is measured relative to the direction of the c.m. velocity vector of the ejected electron and the outgoing proton. We explained the experimentally observed narrowing effect (for *laboratory* scattering angle) by interference effects occurring between the scattering processes corresponding to the first- and second-order term of the Born series.

Considering the relatively large value of the perturbation parameter η, the applicability of the perturbation method for this collision is questionable. The convergence of the Born series could be checked by comparing the results of SBA calculations with those obtained by a nonperturbative quantum-mechanical theory, for example, by applying the recently developed impact parameter coupled pseudostate (CP) approximation of McGovern *et al.* [26]. Although CP is only a one-center theory, that is, it cannot account for PCI between the outgoing projectile and the ionized electron, such a check would be very informative. Furthermore, the analysis

of the separate contributions of f^{B1} and f^{B2} to DDCS$_p$ would give insight into the role of the assumed interference effects.

Also from the experimental side, more accurate measurements are needed to confirm the narrowing of DDCS$_p$ at $\Delta E = 53$ eV observed by Schulz *et al.* [4]. Kinematically complete experiments providing cross sections differential also with respect to the emission angle of the ejected electron would greatly help the general understanding of the collisional breakup of the atomic three-body systems. To the knowledge of the author, no measurements exist for the electron cusp in the case of hydrogen target. The shape of the cusp peak is sensitive to the three-body dynamics; therefore, its detailed measurement would offer a further test of the theoretical models.

ACKNOWLEDGMENTS

The author thanks Michael Schulz for providing numerical data of the experimental and theoretical results of Ref. [4], as well as his valuable comments on the manuscript. This work was supported by the National Information Infrastructure Program (NIIF), the National Scientific Research Foundation, and the National Office for Research and Technology of Hungary (NKTH-OTKA, Grant No. K67719).

APPENDIX: MATHEMATICAL ANALYSIS OF DDCS$_p$

Assuming the separability of the primary proton scattering and PCI between the outgoing electron and proton, DDCS$_p$ can be expressed as

$$\frac{d^2\sigma}{d\Omega_p d(\Delta E)} = \int_{4\pi} \frac{d^3\sigma^{\text{promt}}}{d\Omega_p d\Omega_e d(\Delta E)} F(\theta_p', \Delta E) d\Omega_e. \quad \text{(A1)}$$

Here $d^3\sigma^{\text{promt}}/d\Omega_p d\Omega_e d(\Delta E)$ is a triply differential cross section for the *primary* ionization process in which the proton is scattered with energy loss ΔE in direction $\hat{\mathbf{v}}_p$, and the electron is ejected in direction $\hat{\mathbf{v}}_e$. The scattering may take place on both the electron and the target nucleus. The effect of PCI between the ejected electron and the scattered proton is accounted for by the *enhancement factor* $F(\theta_p', \Delta E)$. The latter function implicitly depends on $\hat{\mathbf{v}}_e$, because θ_p' is measured relative to the direction of $\mathbf{v}_{\text{c.m.}}$, and the latter vector depends on the direction of the electron emission. The enhancement factor is singular at $\theta_p' = 0$ and at value of ΔE corresponding to $v_e = v_p$. (The singularity causes the sharp cusp seen in Fig. 5 for DDCS$'_p$.) The integration over the electron emission angle in the whole 4π solid angle washes out the singularity, and this is the reason why the the narrowing effect is absent in DDCS$_p$.

The ridge seen in Fig. 3(b) in DDCS$_p$ for the case of forward-electron ejection ($\theta_e < 5^\circ$) can be explained by Eq. (A1) as follows. Now we have

$$\frac{d^2\sigma(\theta_e < 5^\circ)}{d\Omega_p d(\Delta E)} = \int_{\theta_e < 5^\circ} \frac{d^3\sigma^{\text{promt}}}{d\Omega_p d\Omega_e d(\Delta E)} F(\theta_p', \Delta E) d\Omega_e. \quad \text{(A2)}$$

Since the integration volume (denoted by $\Delta\Omega_e$) is small, the integral can be well approximated by the product of the integrand taken at an average value of its argument and $\Delta\Omega_e$:

$$\frac{d^2\sigma(\theta_e < 5^\circ)}{d\Omega_p d(\Delta E)} \approx \frac{d^3\sigma^{\text{promt}}}{d\Omega_p d\Omega_e d(\Delta E)}(\theta_p, \langle\theta_e\rangle, \Delta E) \times F(\langle\theta_p'\rangle, \Delta E)\Delta\Omega_e. \quad \text{(A3)}$$

Here $\langle\theta_e\rangle$ is the average value of θ_e in the range $0 < \theta_e < 5^\circ$. $\langle\theta_p'\rangle$ can be estimated as follows. Since the considered angular range of the proton scattering in Fig. 3(b) ($\theta_p < 1$ mrad) is much smaller than the angular range of the electron ejection ($\theta_e < 5^\circ$), therefore $\theta_e' \approx \theta_e$, and thus $\theta_p' \approx (m/M)\theta_e' < 0.05$ mrad. Consequently, $\langle\theta_p'\rangle$ is the average value of θ_p' in the range $0 < \theta_p' < 0.05$ mrad.

Because of the small value of $\langle\theta_p'\rangle$, the enhancement factor in Eq. (A3) is strongly peaked around ΔE corresponding to $v_e = v_p$ (see Fig. 5). Since $F(\langle\theta_p'\rangle, \Delta E)$ does not depend on θ_p, the $v_e = v_p$ peak appears in the same way in the energy-loss spectrum of the scattered proton at each scattering angle, which explains the ridge structure seen in Fig. 3(b).

[1] M. Schulz, R. Moshammer, D. Fischer, H. Kollmus, D. H. Madison, S. Jones, and J. Ullrich, Nature (London) **422**, 48 (2003).
[2] N. Stolterfoht *et al.*, Phys. Rev. Lett. **87**, 023201 (2001).
[3] A. C. Laforge, K. N. Egodapitiya, J. S. Alexander, A. Hasan, M. F. Ciappina, M. A. Khakoo, and M. Schulz, Phys. Rev. Lett. **103**, 053201 (2009).
[4] M. Schulz, A. C. Laforge, K. N. Egodapitiya, J. S. Alexander, A. Hasan, M. F. Ciappina, A. C. Roy, R. Dey, A. Samolov, and A. L. Godunov, Phys. Rev. A **81**, 052705 (2010).
[5] D. S. F. Crothers and J. F. McCann, J. Phys. B **16**, 3229 (1983).
[6] P. D. Fainstein, V. H. Ponce, and R. D. Rivarola, J. Phys. B **24**, 3091 (1991).
[7] A. L. Godunov, Sh. D. Kunikeev, V. N. Mileev, and V. S. Senashenko, Zh. Tekh. Fiz. **53**, 436 (1983).
[8] M. Brauner, J. S. Briggs, and H. Klar, J. Phys. B **22**, 2265 (1989).
[9] R. Dey, A. C. Roy, and C. Dal Cappello, Nucl. Instrum. Methods B **266**, 242 (2008).
[10] A. L. Godunov, V. A. Schipakov, and M. Schulz, J. Phys. B **31**, 4943 (1998).
[11] M. F. Ciappina, W. R. Cravero, and M. Schulz, J. Phys. B **40**, 2577 (2007)
[12] M. Schulz, M. Dürr, B. Najjari, R. Moshammer, and J. Ullrich, Phys. Rev. A **76**, 032712 (2007).
[13] M. Dürr, B. Najjari, M. Schulz, A. Dorn, R. Moshammer, A. B. Voitkiv, and J. Ullrich, Phys. Rev. A **75**, 062708 (2007).
[14] M. F. Ciappina, T. Kirchner, and M. Schulz, Comput. Phys. Commun. **181**, 813 (2010).
[15] T. Vajnai, A. D. Gaus, J. A. Brand, W. Htwe, D. H. Madison, R. E. Olson, J. L. Peacher, and M. Schulz, Phys. Rev. Lett. **74**, 3588 (1995).
[16] M. Schulz, T. Vajnai, A. D. Gaus, W. Htwe, D. H. Madison, and R. E. Olson, Phys. Rev. A **54**, 2951 (1996).

[17] R. Abrines and I. C. Percival, Proc. Phys. Soc. London **88**, 861 (1966).
[18] R. E. Olson and A. Salop, Phys. Rev. A **16**, 531 (1977).
[19] C. O. Reinhold and C. A. Falcón, Phys. Rev. A **33**, 3859 (1986).
[20] C. O. Reinhold and R. E. Olson, Phys. Rev. A **39**, 3861 (1989).
[21] L. Sarkadi and R. O. Barrachina, Phys. Rev. A **71**, 062712 (2005).
[22] C. F. Barnett (editor), *Atomic Data for Fusion*, Oak Ridge National Laboratory Report No. D6, 1990 [http://www-cfadc.phy.ornl.gov/redbooks/redbooks.html].
[23] J. S. Alexander, A. C. Laforge, A. Hasan, Z. S. Machavariani, M. F. Ciappina, R. D. Rivarola, D. H. Madison, and M. Schulz, Phys. Rev. A **78**, 060701(R) (2008).
[24] L. Sarkadi, U. Brinkmann, A. Báder, R. Hippler, K. Tőkési, and L. Gulyás, Phys. Rev. A **58**, 296 (1998).
[25] M. McGovern, Colm T. Whelan, and H. R. J. Walters, Phys. Rev. A **82**, 032702 (2010).
[26] M. McGovern, D. Assafrão, J. R. Mohallem, Colm T. Whelan, and H. R. J. Walters, Phys. Rev. A **81**, 042704 (2010).